Ocean Dynamics (2013) 63:243–263
DOI 10.1007/s10236-012-0589-6

On the dynamics of strait flows: an ocean model study of the Aleutian passages and the Bering Strait

Tal Ezer · Lie-Yauw Oey

Received: 26 June 2012 / Accepted: 19 December 2012 / Published online: 8 January 2013

Abstract A high-resolution numerical ocean circulation model of the Bering Sea (BS) is used to study the natural variability of the BS straits. Three distinct categories of strait dynamics have been identified: (1) Shallow passages such as the Bering Strait and the Unimak Passage have northward, near barotropic flow with periodic pulses of larger transports; (2) wide passages such as Near Straits, Amukta Pass, and Buldir Pass have complex flow patterns driven by the passage of mesoscale eddies across the strait; and (3) deep passages such as Amchitka Pass and Kamchatka Strait have persistent deep return flows opposite in direction to major surface currents; the deep flows persist independent of the local wind. Empirical orthogonal function analyses reveal the spatial structure and the temporal variability of strait flows and demonstrate how mesoscale variations in the Aleutian passages influence the Bering Strait flow toward the Arctic Ocean. The study suggests a general relation between the barotropic and baroclinic Rossby radii of deformations in each strait, and the level of flow variability through the strait, independent of geographical location. The mesoscale variability in the BS seems to originate from two different sources: a remote origin from variability in the Alaskan Stream that enters the BS through the Aleutian passages and a local origin from the interaction of currents with the Bowers Ridge in the Aleutian Basin. Comparisons between the flow in the Aleutian passages and flow in other straits, such as the Yucatan Channel and the Faroe Bank Channel, suggest some universal topographically induced dynamics in strait flows.

Keywords Bering Sea · Aleutian passages · Numerical ocean modeling · Flow–topography interaction · Strait dynamics

Responsible Editor: Yasumasa Miyazawa

This article is part of the Topical Collection on the *4th International Workshop on Modelling the Ocean in Yokohama, Japan 21-24 May 2012*

T. Ezer (✉)
Center for Coastal Physical Oceanography,
Old Dominion University, 4111 Monarch Way,
Norfolk, VA 23508, USA
e-mail: tezer@odu.edu

L.-Y. Oey
Program in Atmospheric and Oceanic Sciences,
Princeton University, Sayre Hall, P.O. Box CN710,
Princeton, NJ 08544-0710, USA
e-mail: lyo@princeton.edu

1 Introduction

The Bering Sea (BS) is located between North America in the east and Asia in the west and between the North Pacific Ocean in the south and the Arctic Ocean in the north (Fig. 1a). The BS is divided between the shallow Bering Shelf in the east and the deep Aleutian Basin in the southwest. The anti-clockwise coastal currents around the Aleutian Basin (Fig. 1b) include the Aleutian North Slope Current (ANSC; Stabeno et al. 2009), the Bering Slope Current (BSC; Johnson et al. 2004), and the Kamchatka Current (KC; Panteleev et al. 2006). South of the BS along the Aleutian Arc, an energetic western boundary current, the Alaskan Stream (Favorite 1967; Reed 1968, 1984; Thomson 1972; Reed and Stabeno 1999), is found (Figs. 1 and 2). There are evidences that the AS influences the flow through the Aleutian passages and the BS circulation (Favorite 1974; Royer and Emery 1984; Reed 1990; Reed and Stabeno 1993; Stabeno and Reed 1992; Stabeno et al. 1999, 2005; Maslowski et al. 2008; Ladd and Stabeno 2009; Ezer and Oey 2010), but the exact mechanism of its influence is not fully understood. North of the BS is the Chukchi Sea that

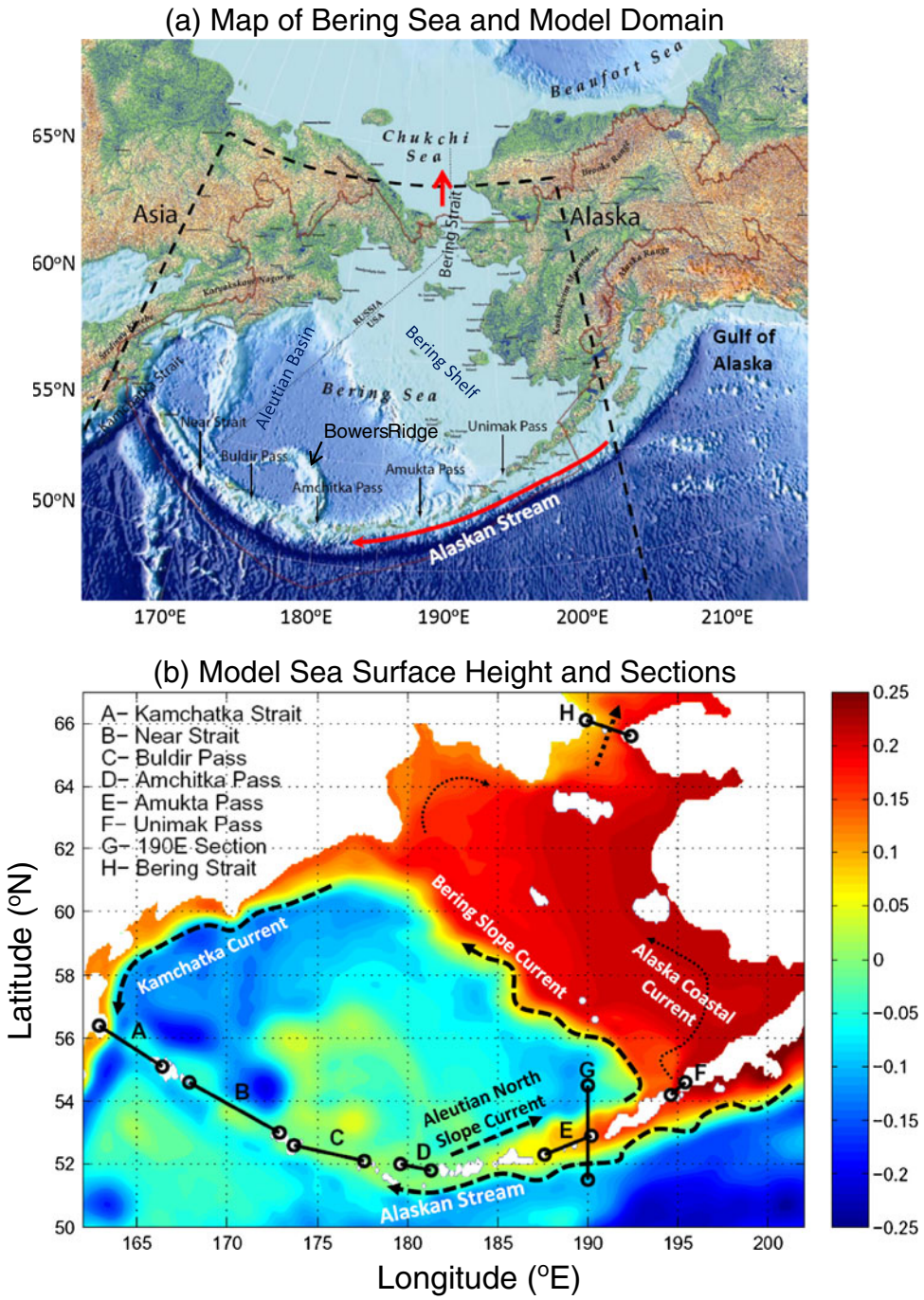

Fig. 1 **a** Map of the area of interest and locations of important passages; the model domain (*dash line*) extends south to about 40°N. **b** Annual mean model sea surface height and schematic of the major currents. Various sections, passages, and straits are marked by "*A*" to "*H*" in (**b**)

leads to the Arctic Ocean. The Bering Strait provides the only connection between the Pacific and the Arctic Oceans, so it plays a crucial role in the global ocean circulation and climate (De Boer and Nof 2004). Long-term observations of the Bering Strait flow indicate variability at a wide range of scales (Aagaard et al. 1985; Coachman and Aagaard 1988; Roach et al. 1995; Woodgate et al. 2005; 2006). The modeling study of Ezer and Oey (2010; hereafter EO10) suggests that some of the variability in the Bering Strait are related to the variability generated in the Pacific Ocean and transferred through the Aleutian Passages; their study shows the need for better understanding of dynamics of strait flow, which motivated the present study.

Global climatic changes and the Pacific Decadal Oscillations (PDO) may influence the ecosystem in the BS (Hunt et al. 2002; Jin et al. 2009). However, it is not clear if the BS–Pacific connection is mostly through air–sea interactions, in which seasonal and interannual variations in the atmosphere over the North Pacific impact the BS (Pickart et al. 2009), or potentially there is also oceanic connections such that, for

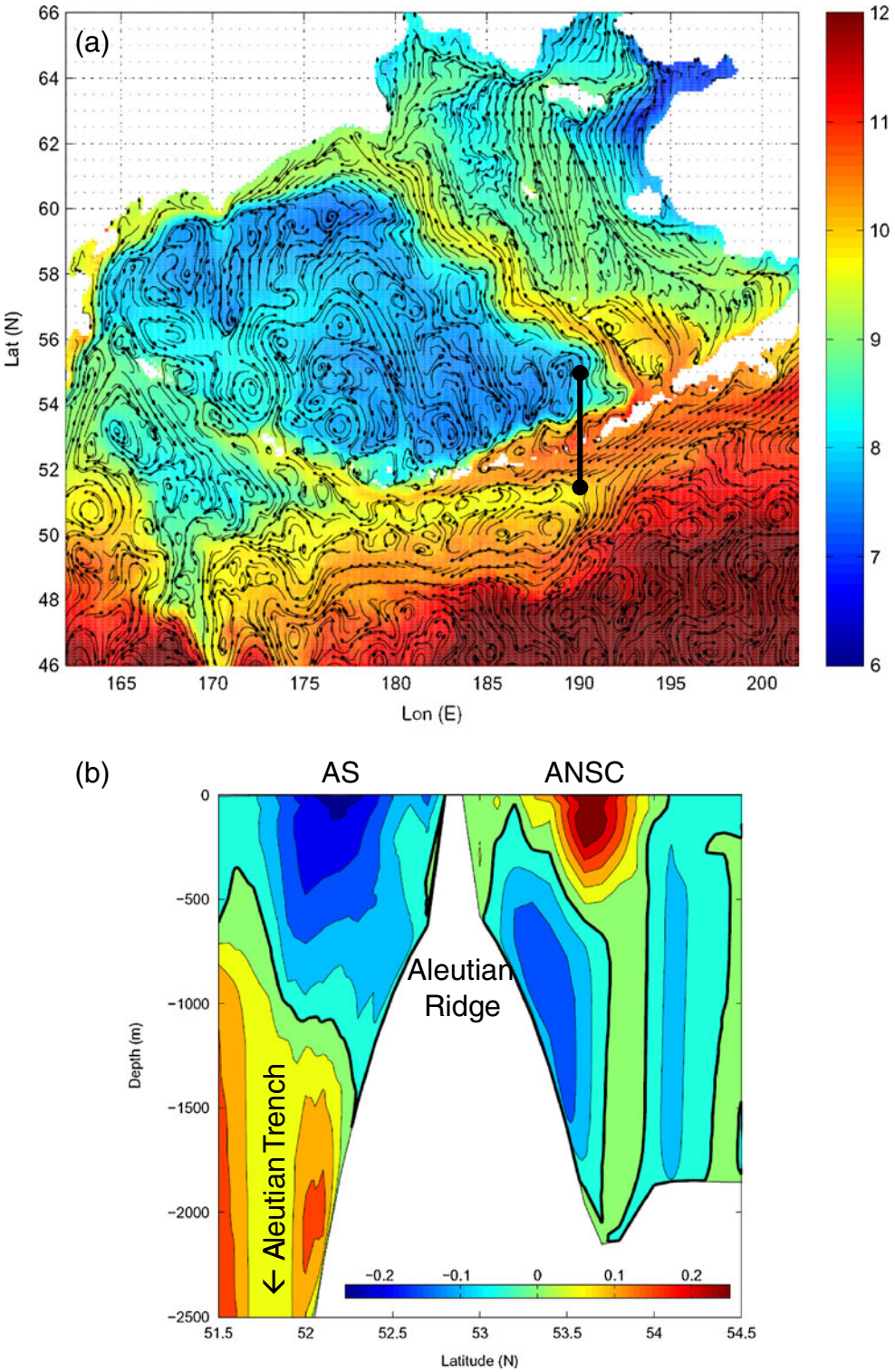

Fig. 2 **a** Surface temperature (degrees Celsius, *in color*) and velocity trajectories obtained from the annual model fields. **b** The mean flow at a north–south section across 190°E (see **a** for location), showing the westward flowing Alaskan Stream (AS, *blue core*) and the eastward flowing Aleutian North Slope Current (ANSC, *red core*) on both sides of the Aleutian Ridge

example, PDO-related variations in circulation in the Gulf of Alaska (Royer 1975) impact the Alaskan Current and associated strait flows into the BS, as suggested by EO10. The exchange of momentum and heat between the Pacific Ocean and the BS is complex, as it involves flows crossing the Aleutian Ridge into the BS through many passages and straits of different geometry. For comparison, other basins are often connected to each other through only a few straits that are more easily monitored; examples are the Bering Strait, Denmark Strait, Faroe Bank Channel, Gibraltar Strait, Yucatan Channel, Florida Strait, etc.

The large variability of the flow in individual passages makes it difficult to estimate the mean flow from sparse

observations, and observations of flows in deep straits often cover only the upper layers. As a result, strait transports reported in the literature sometimes differ by an order of magnitude from each other, and in some cases do not agree on the direction of the mean flow (see a summary of 13 observational studies of strait flows in Table 1 of EO10). Therefore, ocean circulation models are important tools in complementing measurements and in shedding light on the BS circulation and strait flows (Overland et al. 1994; Liu and Leendertse 1982; Wang et al. 2009; Hu and Wang 2010; EO10). We will use here the same ocean circulation numerical model as in EO10, but the focus will be on understanding the intrinsic dynamics of strait flows. Comparing the various BS straits, with their wide range of topographies and geographical locations, could serve as a case study to see if there are any common mechanisms that govern the dynamics of strait flows. For example, the shallow (~70 m) Unimak Pass (see Fig.1a for locations and names of all passages analyzed in this study) in the east has northward flow directly into the Bering Shelf, to feed the Alaskan Coastal Current (Fig. 1b), but on the other (western) end of the Aleutian Arc is the deep (~4,500 m) Kamchatka Strait (Panteleev et al. 2006), with a southward surface flow of the KC toward the Pacific. Although these two straits are connected through complex current systems

Table 1 Characteristics of straits and passages in the BS unforced model, ordered by decreasing aspect ratio ("*s*" in third column) and labeled by the three categories discussed in the text

Strait/passage	Longitude, latitude	$s = \frac{L(\mathrm{km})}{H(\mathrm{km})}$	V (ms^{-1}) ΔH (m) g' (ms^{-2})	R^T (km) R^C (km) Fr	L/R^T L/R^C B	Transport SD/mean (in Sv)
"Shallow" straits						
Bering Strait	169.9°W, 65.7°N	~85/0.05=~1,700	V~0.2 ΔH~20 g'~0.0007	R^T~170 R^C~1 Fr~1.6	L/R^T~0.5 L/R^C~85 B=0.07	0.09/0.35=~0.26
Unimak Pass	165.2°W, 54.3°N	~50/0.07=~700	V~0.5 ΔH~25 g'~0.007	R^T~260 R^C~3.5 Fr~1.2	L/R^T~0.2 L/R^C~14 B=0.06	0.21/0.47=~0.45
"Wide" straits						
Amukta Pass	172.0°W, 52.5°N	~250/0.75=~330	V~0.1–0.2 ΔH~50 g'~0.007	R^T~720 R^C~5.1 Fr~0.1	L/R^T~0.35 L/R^C~49 B=0.46	0.69/1.2=~0.58
Buldir Pass	184.2°W, 52.4°N	~350/1.5=~230	V~0.1–0.5 ΔH~100 g'~0.007	R^T~1,050 R^C~7.3 Fr~0.4	L/R^T~0.33 L/R^C~48 B=0.51	1.2/4.1=~0.29
Near Strait	190.0°W, 54.0°N	~500/3.5=~150	V~0.1–0.5 ΔH~100 g'~0.007	R^T~1,330 R^C~7.3 Fr~0.4	L/R^T~0.38 L/R^C~68 B=0.53	3.2/2.64=~1.21
"Deep" straits						
Amchitka Pass	180.0°W, 51.8°N	~120/1.8=~65	V~0.1–0.2 ΔH~100 g'~0.007	R^T~1,050 R^C~7.3 Fr~0.2	L/R^T~0.1 L/R^C~16 B=0.48	0.78/3.2=~0.24
Kamchatka Strait	195.0°W, 56.0°N	~200/4.5=~45	V~0.5–1 ΔH~200 g'~0.007	R^T~1,740 R^C~9.8 Fr~0.6–1	L/R^T~0.1 L/R^C~20 B=0.32	5.5/1.1=~5
Other straits						
Faroe Bank Channel	6.0°W, 60.0°N	~20/0.8=~25	V~0.5–1 ΔH~200 g'~0.007	R^T~700 R^C~20 Fr~0.6–1	L/R^T~0.03 L/R^C~1	1.5/3=~0.5
Yucatan Channel	85.8°W, 21.5°N	~150/2=~75	V~1–1.5 ΔH~200 g'~0.03	R^T~2,600 R^C~40 Fr~0.3	L/R^T~0.06 L/R^C~4	5/30=~0.17

Data from models of the Faroe Bank Channel (Ezer 2006) and the Yucatan Channel (Ezer et al. 2003) are also shown. L and H are the width and maximum depth, respectively. V and ΔH are upper layer velocity and thickness, and g' is the reduced gravity. R^T and R^C are the barotropic and baroclinic Rossby radii of deformation. Fr is the baroclinic Froude Number. B is the baroclinic factor, whereas a purely barotropic flow (depth independent) will have B~0, and a purely baroclinic flow with zero net flow will have B~1. See text for definitions of all variables

(Fig. 1b), one may ask if there is anything in common between these two straits and the way in which they influence the BS variability. Even without any time-dependent forcing, the BS model of EO10 shows energetic mesoscale variability in all straits. Therefore, some open questions are as follows: what is the source of the variability and how do parameters such as stratification, topography, and geographical location impact the flow pattern and variability in these straits?

Comparative studies of strait flows, such as the Gravity Current Entrainment Climate Process Team (GCE/CPT) project (Legg et al. 2009), which involved regional and global models, laboratory experiments, process studies, and observations, attempted to characterize the dynamics in different straits around the globe by comparing a few basic parameters; we will try to compare the BS straits in a similar manner here. While some limited model–data comparisons are included in EO10, the main purpose of the present process-oriented model study is not to produce realistic simulations, but to isolate the natural variability of the BS and understand basic mechanisms; for more realistic simulations of the circulation and sea ice in the BS, see for example the model studies of Wang et al. (2009) or Hu and Wang (2010). Therefore, the model simulations intentionally omit sea ice as well as tides (Foreman et al. 2006) and focus on mesoscale variability generated by the internal circulation dynamics without surface forcing; these results are also compared with a simulation that includes wind forcing. The study follows on the footsteps of similar process studies of straits dynamics by the authors, such as the studies of the Yucatan Channel (YC) between the Caribbean Sea and the Gulf of Mexico (Ezer et al. 2003; Oey et al. 2004) and the study of the Faroe Bank Channel (FBC) between the Arctic and the North Atlantic Ocean (Ezer 2006). Comparisons between the dynamics of the Aleutian passages and other straits (e.g., YC and FBC) located in different oceans with very different conditions may show if there are some common characteristics of strait dynamics.

The goals of the study are twofold: first, to use the BS straits as a case study to understand general characteristics of strait dynamics and, second, to shed light on how and where mesoscale variability is generated and distributed in the BS. The paper is organized as follows: Section 2 describes the model setting, Section 3 analyses various aspects of the model results, and Section 4 offers a discussion and conclusions.

2 The Bering Sea model setting

The model used here is the same as in EO10, and we analyze the experiment described there as AS=25 Sv (imposed Alaskan Stream transport of 25 Sv; 1 Sv=$10^6 m^3 s^{-1}$). The focus of the study is on "natural" mesoscale variability in a model simulation without surface forcing. However, limited comparisons are also made with a simulation that includes six-hourly surface winds obtained from QuikScat (http://rda.ucar.edu/datasets/). Note that discussions that do not indicate a "wind-driven" case are assumed to refer to the standard unforced case. The numerical model is based on the Princeton Ocean Model (POM) code (Mellor 2004; for the latest version, see www.aos.princeton.edu/WWWPUBLIC/htdocs.pom/), which is a terrain-following (sigma coordinates), free surface, primitive equation ocean circulation model with the Mellor and Yamada (1982) turbulence closure scheme. The horizontal model resolution is (Δx, Δy)~(5, 8 km), and the vertical grid has 51 sigma layers ($\sigma=(z-\eta)/(H+\eta)$, where −H (bottom)$<z<\eta$ (surface elevation)). The model domain is shown in Fig. 1a. A constant inflow transport of 25 Sv is imposed on the eastern boundary where the Alaskan Stream enters the domain from the Gulf of Alaska. Of this transport, 24.5 Sv exits the western boundary of the model, and 0.5 Sv exits through the northern boundary to the Chukchi Sea north of the Bering Strait. The rest of the open boundaries have radiation boundary conditions. Note that the northward transport is somewhat less than estimates of the Bering Strait mean transport of ~0.8 Sv, since the model neglects contributions from freshwater and wind-driven forcing. Due to interannual variations in the Bering Strait transport, there are years when transports less than ~0.6 Sv (i.e., similar to the model transport) are observed (Aagaard et al. 1985). The analysis presented here is based on 1-year daily output, starting after 12 years of spin-up simulation. For more details on the model, see EO10.

Figure 2 shows the mean surface temperature and currents, as well as the vertical structures of AS and ANSC. Figure 3 shows the daily transport in seven straits and passages during a 1-year simulation following the spin-up. It is interesting to note how rich spatial (Fig. 2) and temporal (Fig. 3) variability can exist in a model that has no time-dependent forcing. In several straits (e.g., Near and Kamchatka Straits), the standard deviation is larger than the mean flow, indicating the difficulty of estimating the mean flow from short-term observations. The mesoscale variability seems quite chaotic, and different patterns are seen in each strait, so in the next sections, further analysis is conducted in order to quantify the dominant modes of variability and their sources.

3 Results

3.1 Characteristics of the straits

To distinguish between the different straits, a series of parameters that characterize the topography, stratification, and flow variability are estimated from the model and summarized in Table 1; some of these parameters are shown in Fig. 4. They include the following:

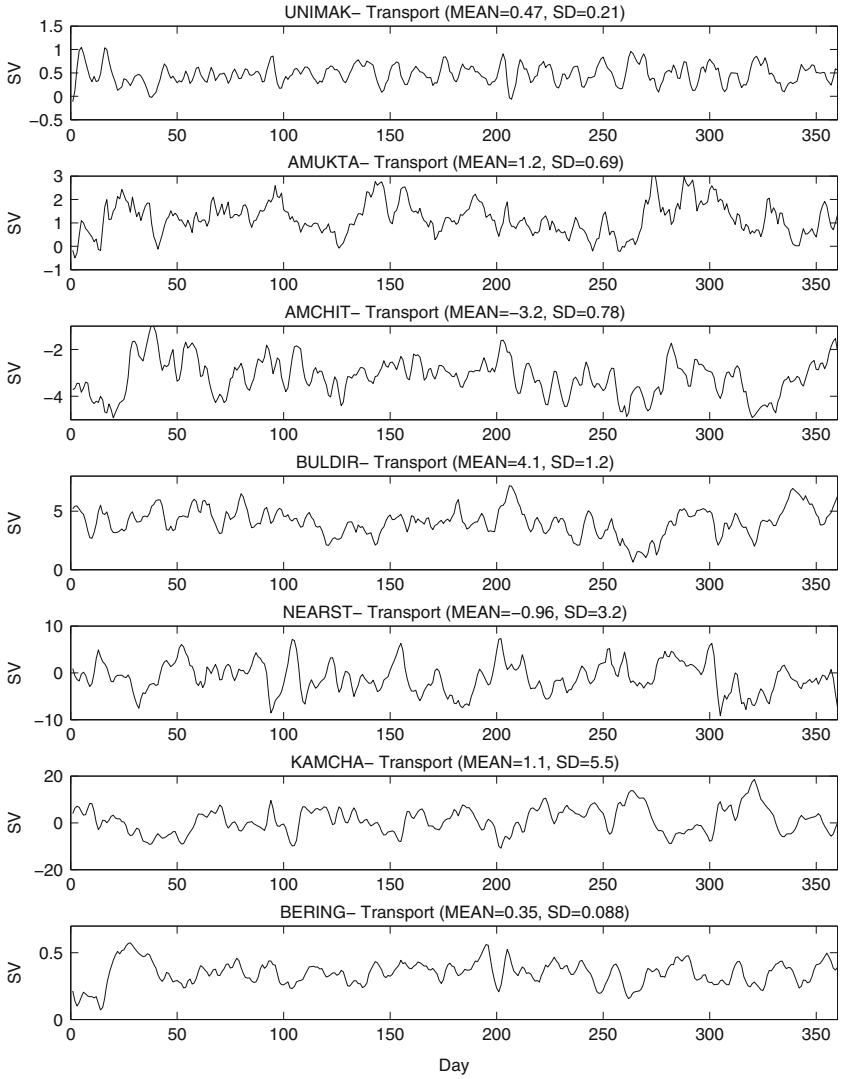

Fig. 3 Transport variations through Bering Sea passages (from *top to bottom*: Unimak Pass, Amukta Pass, Amchitka Pass, Buldir Pass, Near Strait, Kamchatka Strait, and Bering Strait) for the 13th year of simulation without any time-dependent forcing. Mean transport (in Sverdrup) and standard deviation are indicated in each panel; note the different vertical scale for each panel

The aspect ratio,

$$s = \frac{\text{strait width(L)}}{\text{strait depth(H)}}, \tag{1}$$

the barotropic and baroclinic Rossby radii of deformation,

$$R^T = \frac{\sqrt{gH}}{f}; \quad R^C = \frac{\sqrt{g'\Delta H}}{f}, \tag{2a, b}$$

the baroclinic Froude number and the reduce gravity parameter,

$$\mathrm{Fr} = \frac{\mathrm{V}}{\sqrt{\mathrm{g}'\Delta \mathrm{H}}}; \quad \mathrm{g}' = \mathrm{g}\frac{\Delta\rho}{\rho_0}, \tag{3a, b}$$

where g is the gravity constant, f is the Coriolis parameter, V and ΔH are the velocity and thickness of the upper layer, respectively, and $\Delta\rho/\rho_0$ is the ratio between the density change across layers and a reference mean density. R^T and R^C represent the dynamic scales of motions and Fr the stability (see Ezer 2006, for the impact of Fr on the Faroe Bank Channel flow, and Legg et al. 2009, for the value of these parameters in various straits with overflow gravity currents). Another parameter is the "Baroclinic Factor," B, which shows how much the strait's time-mean flow, $v(x, z)$, deviates from the vertically averaged flow, $\overline{v}^z(x)$; it is defined as

$$B = \frac{1}{L}\int_{x=0}^{L}\left[\frac{\int_z [v(x,z)-\overline{v}^z(x)]^2 dz}{\int_z [v(x,z)]^2 dz}dx\right]; \quad \overline{v}^z(x) = \int_{z=-H}^{0} v(x,z)dz. \tag{4}$$

Pure barotropic flows with no shear will have $B \sim 0$, while baroclinic flows, say two layers flowing in opposite directions and exactly balancing each other's transport, will have $B \sim 1$. It is immediately evident (Table 1 and Fig. 4c) that the flow in the shallowest two straits (Bering and Unimak) tends to be more barotropic ($B \sim 0.06$) than the flow in the wide and deep straits (where $B \sim 0.5$); thus, the wide and deep straits allows more vertical variations in currents throughout the water column.

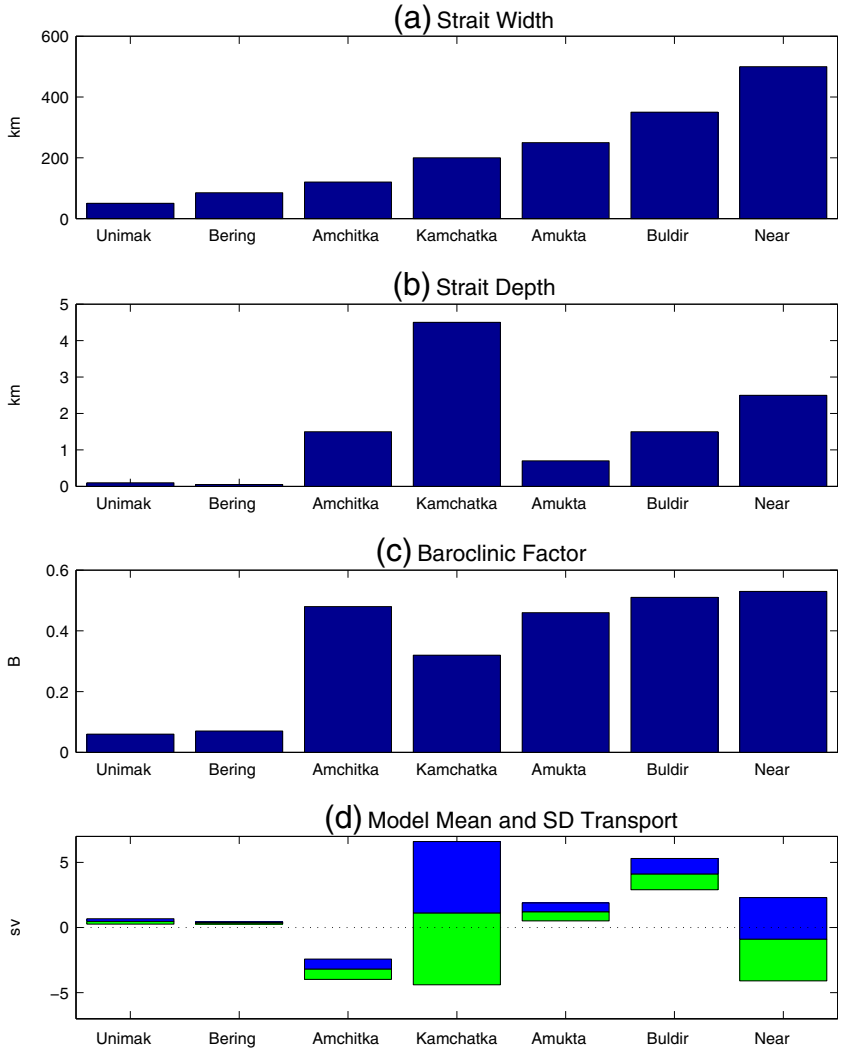

Fig. 4 The characteristics of the Bering Sea straits: (**a**) width, (**b**) maximum depth, (**c**) baroclinic factor B (see text), and (**d**) transport variability; mean±standard deviation (idealized case with no surface forcing)

The barotropic radius of deformation, which depends on depth H (Eq. 2a), is smaller ($R^T \sim 200$ km) in the shallow straits than in the deeper straits ($R^T \sim 1{,}000$ km), but since the shallow straits are also narrower, in all the straits, R^T is larger than the strait's width by a factor of 2 to 10. The baroclinic radius (R^C, Eq. 2b), on the other hand, is smaller than L in all cases, allowing baroclinic variability to propagate across the straits. Table 1 also compares the BS passages with the Faroe Bank Channel (FBC) data from Ezer (2006) in the North Atlantic and with the Yucatan Channel (YC) data from Ezer et al. (2003) in the Caribbean Sea. Because of the strong stratification in the FBC, g' is relatively large, and $R^C \sim 20$ km. In the YC, strong stratification and low latitude (small f) result in $R^C \sim 40$ km (Ochoa et al. 2001); the baroclinic Rossby radii in FBC and YC are thus larger than those found in the BS straits (1–10 km). In the wider Aleutian straits, $L/R^C \sim 50$, while in the YC and the FBC, $L/R^C \sim 1$–4. Therefore, one expects the wide Aleutian straits to allow baroclinic mesoscale features to propagate across the strait; evidence for such eddies is shown later. In comparison, the narrow FBC is dominated by strong along-channel flow with little or no signal of cross-channel propagation, but the wider YC may have some evidence of baroclinic eddies propagating across the channel (Ochoa et al. 2001; Sheinbaum et al. 2002). The comparison of BS passages with other straits is included here to show the generality of straits dynamics.

The (unforced) flow variability in the model (Fig. 4d) is especially large in the deepest strait (Kamchatka Strait) and in the widest strait (Near Strait); both are located in the western side of the Aleutian ridge. Nevertheless, the spatial and temporal flow pattern in those straits is very different.

EO10 compared some of the mean and variability of the strait flow (Table 1 and Fig. 4) with observations. While model–data comparison is beyond the scope of this study, it is important to emphasize that there is large discrepancy between various observations due to mesoscale variability, and in fact, in many straits, the standard deviation of transports is large compared with the mean (Fig. 4d). Discrepancy between the model and observations also arose

due to the idealized nature of the model (the "standard" case omits wind, sea ice, and tides). For example, the model underestimated southward transport in Kamchatka Strait (Panteleev et al. 2006), which can be partly attributed to the southward seasonal wind pattern along the coast of Asia (Pickart et al. 2009). While the KC in the upper west side of the Kamchatka Strait is quite realistic in the model, the net simulated transport in the strait is small because of strong northward deep flow that balances the southward KC flow; there are currently no direct current meter observations in the deepest part of the Kamchatka Strait to verify if these deep currents in the model exist or not. The Bering Strait flow may also have a wind-driven component (Coachman and Aagaard 1988; Woodgate et al. 2005). On the other hand, the idealized model forcing allows us to focus on the unforced "natural" modes of variability; their spatial and temporal patterns are discussed in the next sections.

What parameters control the "natural" variability of the flow? Figure 5 shows that the variability is increasing monotonically with both the barotropic and the baroclinic Rossby radii, independent of geographical location in the BS or the existence of major ocean currents. Therefore, the local topography (i.e., R^T depends on depth H) and stratification (i.e., R^C depends on change in density $\Delta\rho$ and upper layer thickness ΔH) seem important. Except for the two deepest straits, Near and Kamchatka, the flow variability seems almost linearly correlated with R^T and R^C. For the deepest straits, there seem to be a threshold value of R^T and R^C when variability increases much faster. The impact of Fr is not as clear, with some straits (Unimak and Bering) showing the potential for development of supercritical flow (Fr>1), but in most other straits, subcritical flows (Fr<1) are expected. The laboratory experiments of Cenedese et al. (2004) and the Faroe Bank Channel model simulations of Ezer (2006) show that supercritical overflows may show periodic pulses of larger transports, while for 0.4<Fr<0.6, an "eddy" regime may be found with less regular oscillation and the development of downstream eddies; it will be shown later, that by and large, the strait flow agree with the above flow's descriptions.

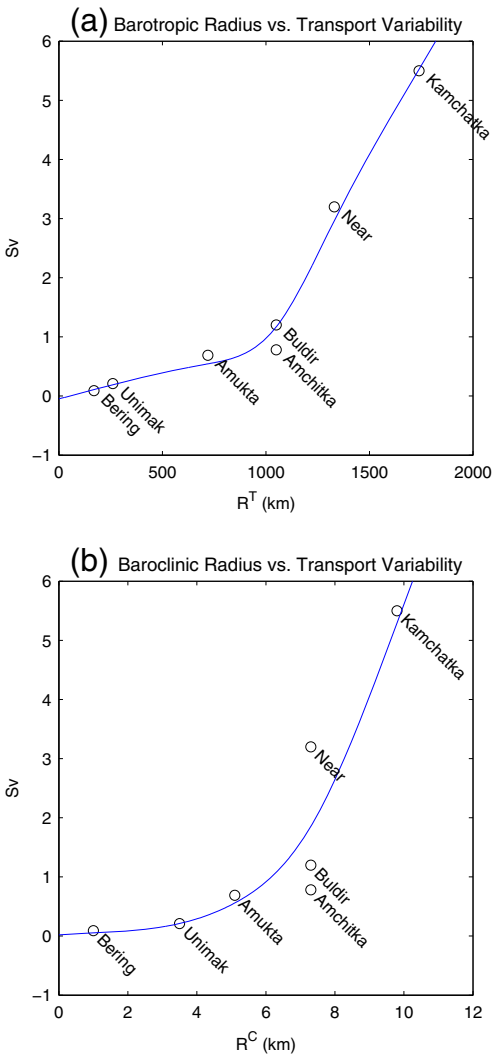

Fig. 5 The transport variability of the various passages versus (**a**) the barotropic radius of deformation and (**b**) the baroclinic radius of deformation. The *blue line* is a smoothed fitting curve

3.2 Categories of strait flow

The apparent strong influence of bottom topography on strait flow (Figs. 4 and 5a) leads us to suggest three categories of strait dynamics, independent of geographical location and forcing:

1. "Shallow" straits (aspect ratio s>500; depth H<100 m), such as the Bering Strait and the Unimak Pass, have near barotropic flow, i.e., the flow does not change much vertically for most of the upper water column, but horizontally, stronger flows are locked at particular locations across the strait (Fig. 6a, c). Temporal variability includes episodic pulses of larger transports (Fig. 6b, d); these mesoscale eddy variations are often associated with supercritical flows (Fr close to or larger than 1; see Table 1). Note that the narrow FBC has a supercritical flow that generates nearly periodic downstream "pulses" (Ezer 2006), somewhat similar to the pattern seen here.
2. "Deep" straits (s<100; H>1,500 m), such as Amchitka Pass and Kamchatka Strait, have major surface currents at the western side of the strait and deep flows along the slopes of the strait (Fig. 7a, c). The core flows meander slightly across the strait, but remain largely locked to topography (Fig. 7b, d). Comparing the mean flow of the "unforced" case (Fig. 7c) to the "wind-driven" case (Fig. 7e) shows surprisingly small differences; the wind intensifies the KC (on the upper left side of the

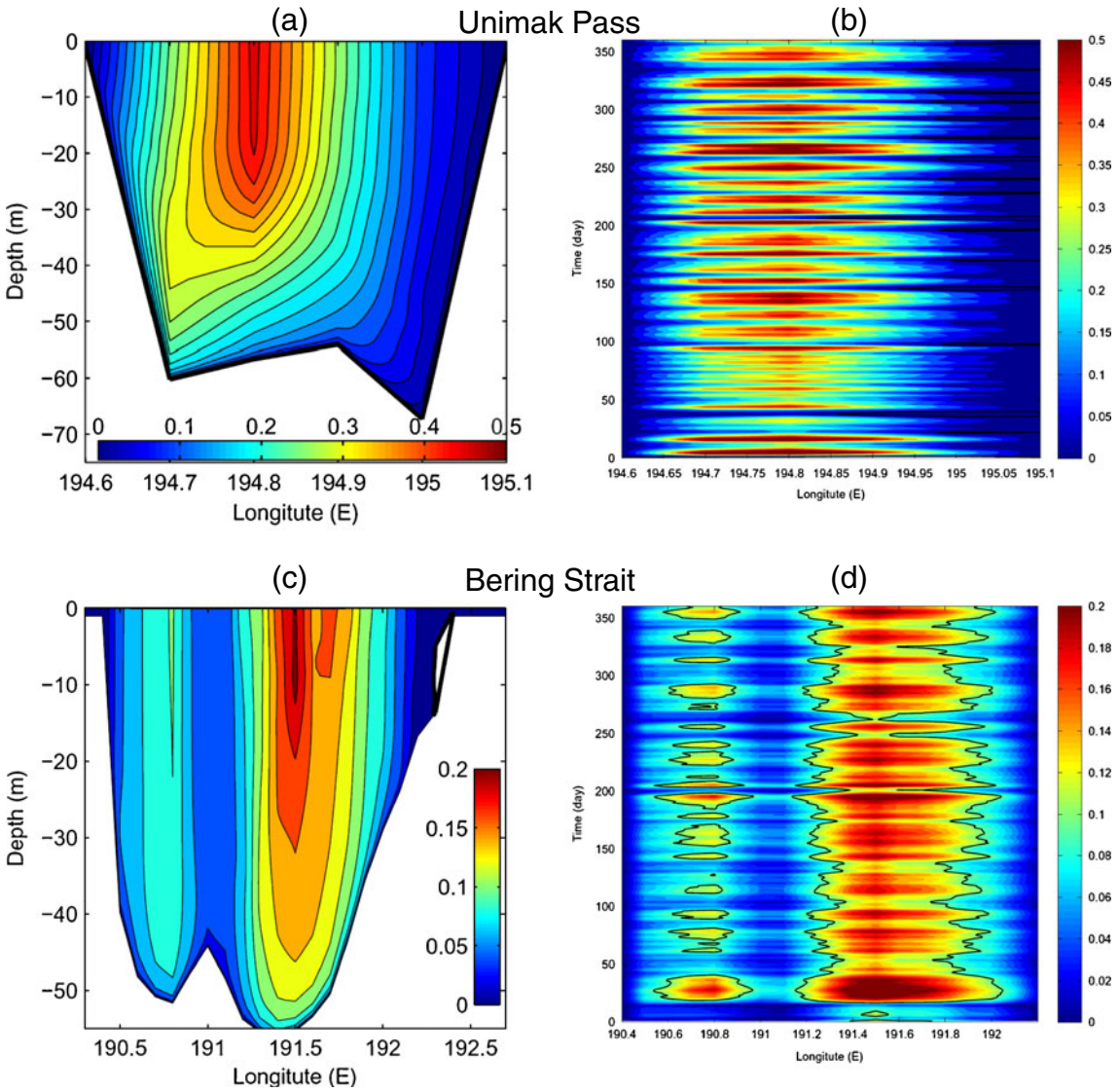

Fig. 6 Cross-section (x–z) of the annual mean flow (in meters per second; *left panels*) in the so-called "Shallow" straits and the vertically averaged flow variability as a function of time and longitude (*right panels*) for the unforced case. From *top to bottom* are the Unimak Pass and the Bering Strait

Kamchatka Strait), but the deep flows remain almost unchanged, indicating the dominant role that topography plays. The Yucatan Channel (YC) belongs to this category in terms of its deep topography (H~2,000 m) and largely resembles this kind of flow (Fig. 7f), with deep flows locked to topography (Ezer et al. 2003). Note that long-term direct current measurements at depths of 1,500–4,500 m in the Aleutian Passages are not available to verify the deep model-simulated flow variability, but some indirect evidence for such flows exist (EO10).

3. "Wide" straits ($100<s<500$; $750\ \text{m}<H<3{,}500$ m), such as Amukta and Buldir Passes and Near Strait, do not have well-organized currents (Fig. 8a, c, e), but are largely influenced by mesoscale eddies that propagate across the strait (Fig. 8b, d, f). The influence of eddies can explain why observations taken at different times often show conflicting flow pattern results (Stabeno and Reed 1992; Reed and Stabeno 1993). Note that eddy signal propagation is westward (Fig. 8b, d) in the Amukta and Buldir Passes (influenced by the westward flowing Alaskan Stream), but is eastward (Fig. 8f) in the Near Strait (probably influenced by BS eddies north of the strait; Figs. 1b and 2a).

Comparisons of model and estimated transports from observations were conducted by EO10. Detailed velocity comparisons are not possible due in part to a lack of full-depth measurements in most straits; the general simulated flow pattern seems reasonable however. For example, the model in Amukta Pass shows that the near-surface

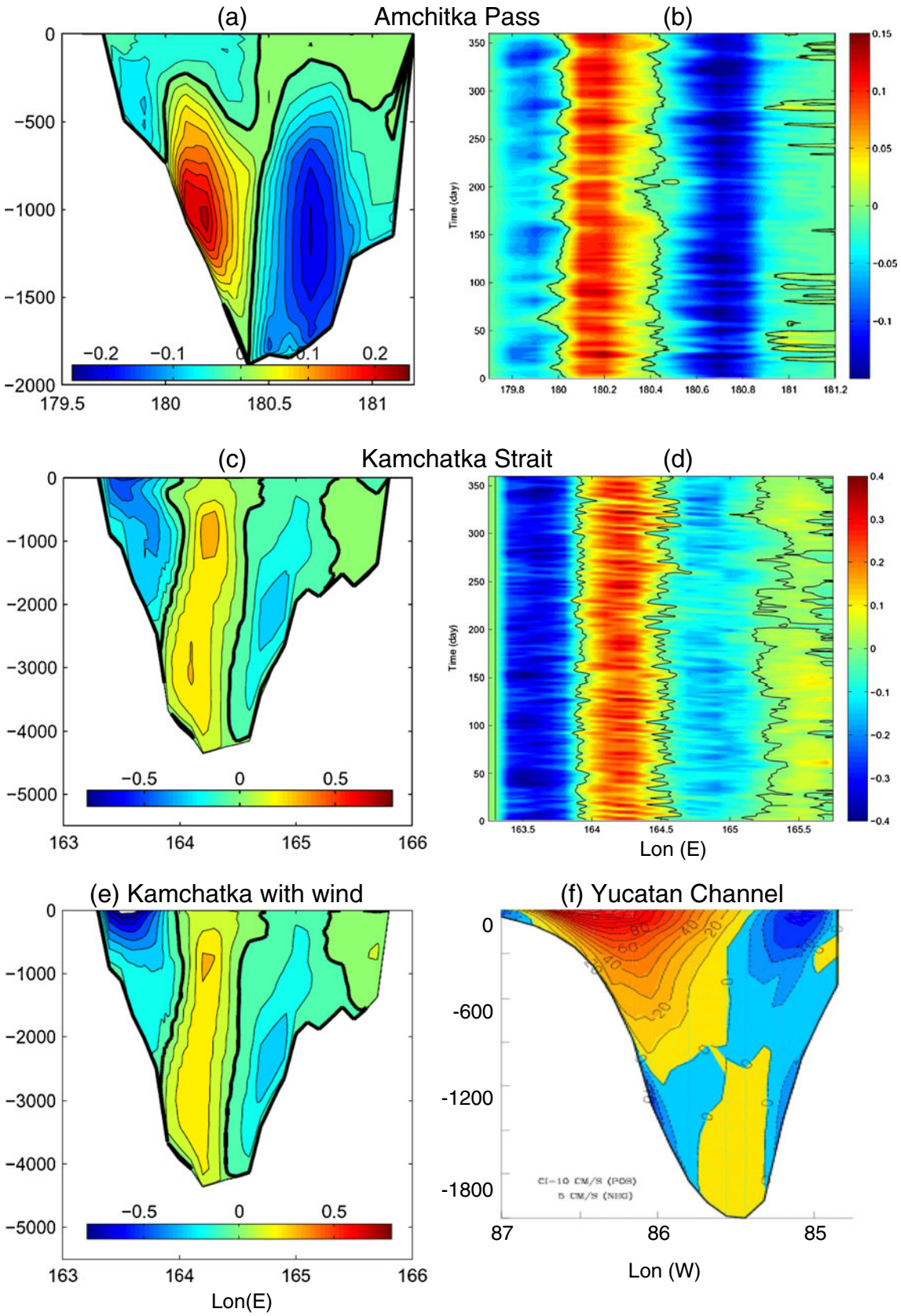

Fig. 7 The *top* and *middle panels* (**a**–**d**) are the same as Fig. 6, but for the so-called "Deep" straits, the Amchitka Pass, and the Kamchatka Strait. The mean flow in Kamchatka Strait for the wind-driven case is shown in (**e**), and the flow in the Yucatan Channel (YC) model of Ezer et al. (2003) is shown in (**f**)

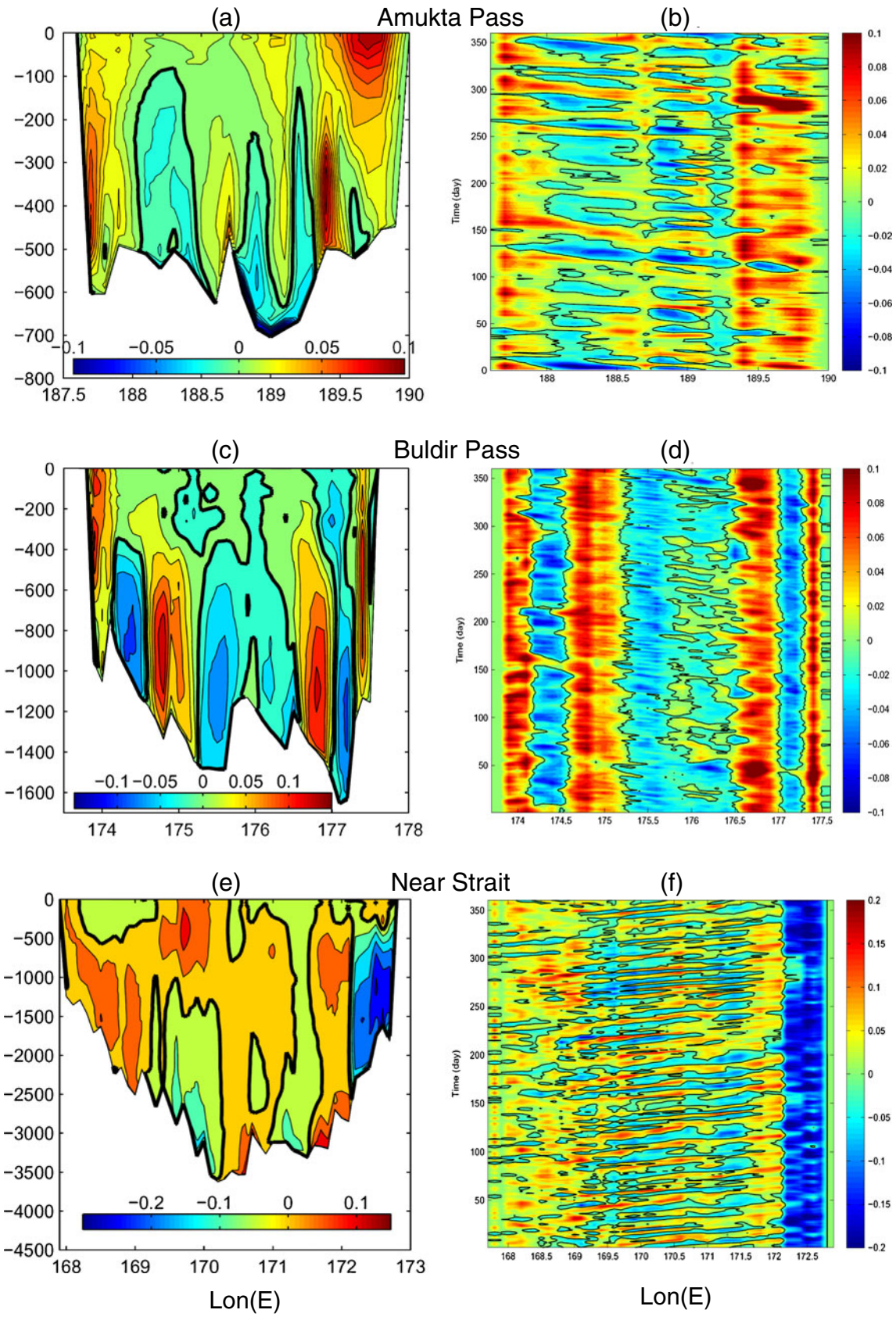

Fig. 8 Same as Fig. 6, but for the so-called "Wide" straits, the Amukta Pass, the Buldir Pass, and the Near Strait

northward flow is intensified in the eastern side of the pass (Fig. 8a), which agrees well with observation (Stabeno et al. 2005, see their Fig. 11a). Moreover, the observed flow in the upper 400 m is more stable in the eastern side of the straits, but more variable with return southward flows in the center and the western sides of the pass (Fig. 12 in Stabeno et al. 2005), as are seen also in Fig. 8a. A strong influence of AS eddies on the Amukta Pass flow is suggested by the observations, which we also see in the model results (Fig. 8b).

3.3 EOF analysis of strait flow: spatial modes and temporal variability

Empirical orthogonal function (EOF) analysis (Bretherton et al. 1992) is a method for analyzing space–time data to uncover spatial patterns and their temporal variability; the method has been used, for example, to study the variability in the Yucatan Channel flow (Ezer et al. 2003; Oey et al. 2004). One year, daily, along strait flow, $V_i(x, z, t)$, where i= 1–7 represents each one of the seven straits (Table 1), x is the distance across the strait ($0<x<L_i$), and z is the depth ($-H_i(x)<z<0$), were used to calculate the first ten EOF modes. Each EOF mode, n, is represented by a spatial pattern, $\Psi_i^n(x, z)$, time series of its amplitude, $A_i^n(t)$, and the percent of variability it represents, $P_i^n(t)$.

Figure 9 summarizes the contribution to the total variability from the first ten modes, from mode-1 (blue) to mode-10 (red). It is quite clear that the "Shallow" straits are very different than the other straits, whereas 90 % and 96 % of the total variability are represented by the first mode in the Unimak Pass and the Bering Strait, respectively; the spatial pattern Ψ_i^1 of mode-1 in these two straits is almost identical to the flow pattern (Fig. 6), and the time variability, A_i^1, is almost identical to the total transport (Fig. 3), so they are not shown. In the other ("Deep" and "Wide") straits, the flow pattern is much more complex, so even ten EOF modes can only represent 60–85 % of the total variability (Fig. 9). Figure 10 shows, for example, the first three EOF modes at the "Deep" straits. At Amchitka Pass, mode-1 primarily represents mid-depth ($z\sim-800$ m; 23 % of the total variability) flow variability, mode-2 represents the surface flow near the western coast, and mode-3 represents the near-bottom deep flows and some possible coupling with the surface (Fig. 10a, c). In Kamchatka Strait, on the other hand, the first two modes represent mid-to-deep flows near the center of the Strait (combining for 26 % of the variability), while only ~9 % of the variability is associated with the KC near the westward coast and represented by mode-3. As indicated in EO10, and shown in Fig. 7e, the simulated KC in the unforced model is somewhat underestimated due to the omission of wind-driven effects.

Buldir Pass and Near Strait are located in the same region on the western part of the Aleutian Island Arc (Fig. 1), but the EOF analysis reveals that they have very different dynamics (Fig. 11). The deep flows are fairly barotropic (see also Fig. 8), and they oscillate at different frequencies, with long periods ($T\sim43$ days), irregular pattern in Buldir Pass (Fig. 11b), but very regular, higher frequency oscillations ($T\sim12$–18 days, see later) in Near Strait (Fig. 11d). The explanation is that Buldir Pass is affected by the Alaskan Stream to the south (where eddies propagate westward), while Near Strait is affected by eddies propagating eastward north of the strait (Fig. 2a); Fig. 8 confirms the different propagation direction.

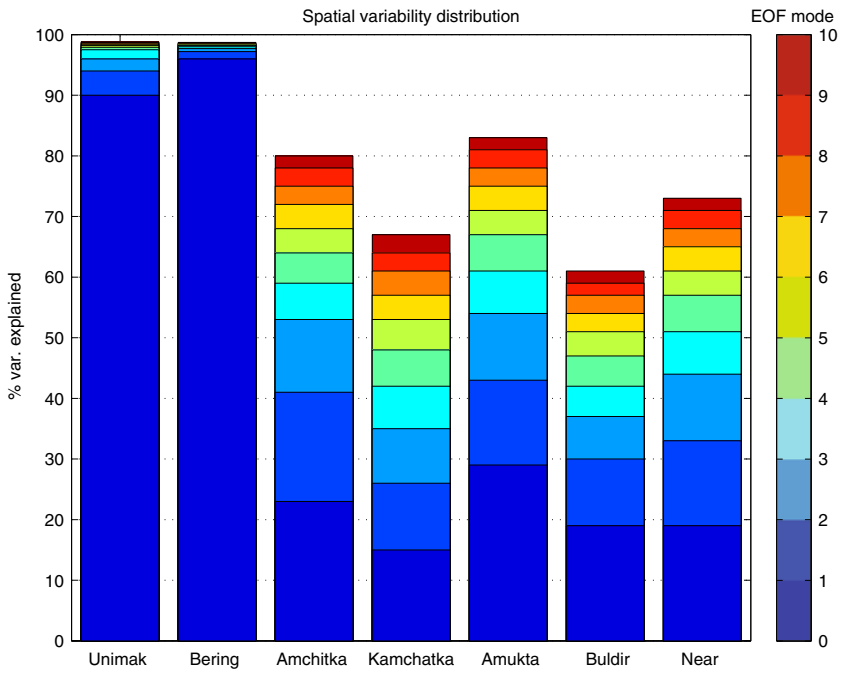

Fig. 9 The spatial variability of the daily flow across seven passages as projected on ten EOF modes (unforced case). The percentage of variability explained by each EOF mode is shown by *colors* (from the first mode in *blue* to the tenth mode in *red*); the *height of each bar* represents the variability explained by the first ten modes

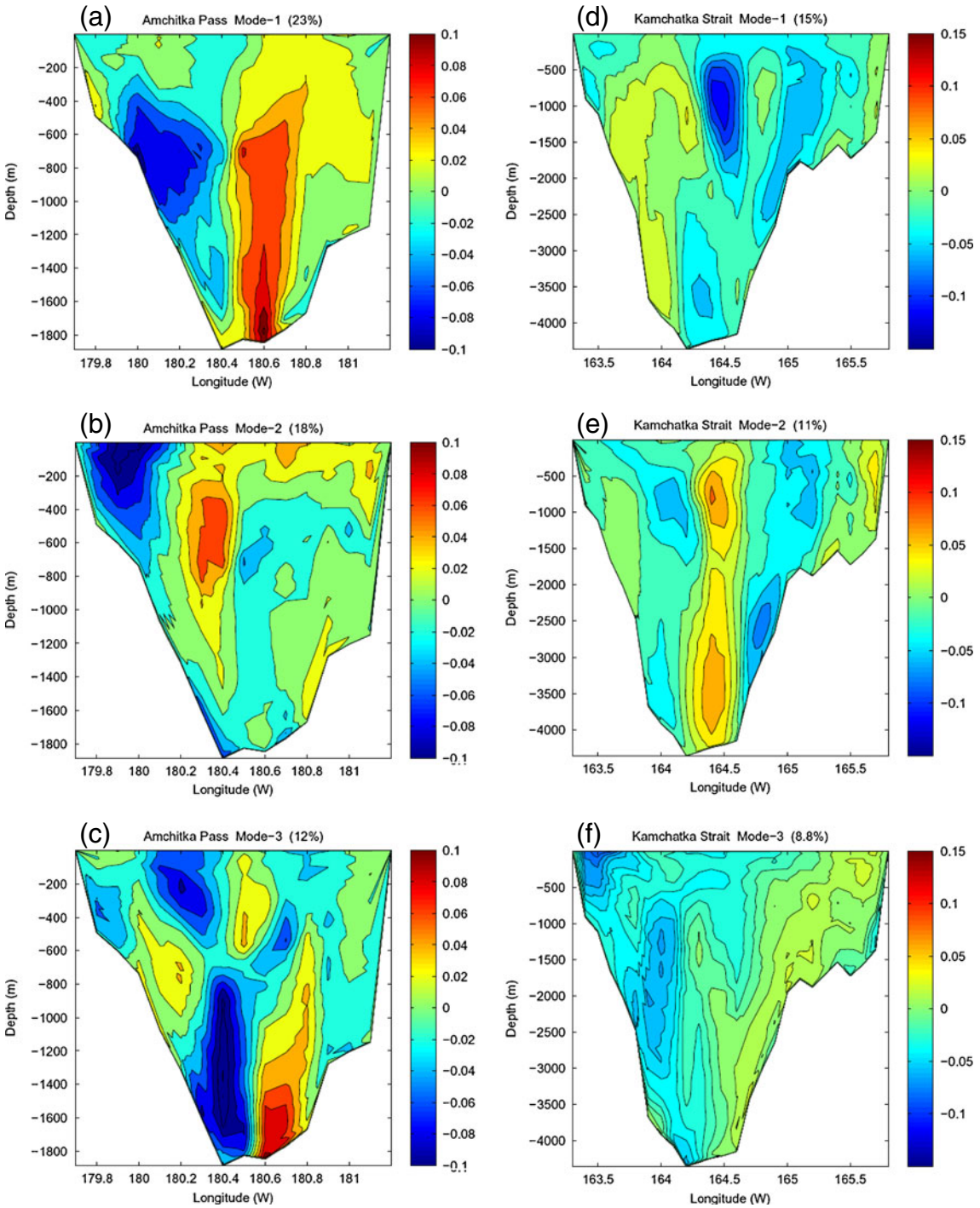

Fig. 10 The spatial pattern of the first three EOF modes in Amchitka Pass (*left panels*) and Kamchatka Straits (*right panels*). The percentage of variability of each mode is indicated in each panel

The dominant periods of the first EOF modes in six straits are calculated by power spectral analysis of $A_i^l(t)$ and shown in Fig. 12. Note that for Kamchatka Strait, modes-1 and -2 are combined, as they both represent the same deep flows and have the same periods. Buldir Pass is not shown, but it is dominated by a 43-day period as Amikta and Amchitka Passes. Dominant periods of strait oscillations include high-frequency modes (T∼5–8 days) that seem to be generated near the Unimak Pass (Fig. 12f), mid-frequency oscillations (T∼12–18 days) which are most prominent in Near Strait (Fig. 12e), and two distinct oscillations, one with T=32 days (Bering and Kamchatka Straits, Fig. 12a, b) and one with T=43 days (Amukta, Amchitka, and Buldir Passes). So, what are the sources of these

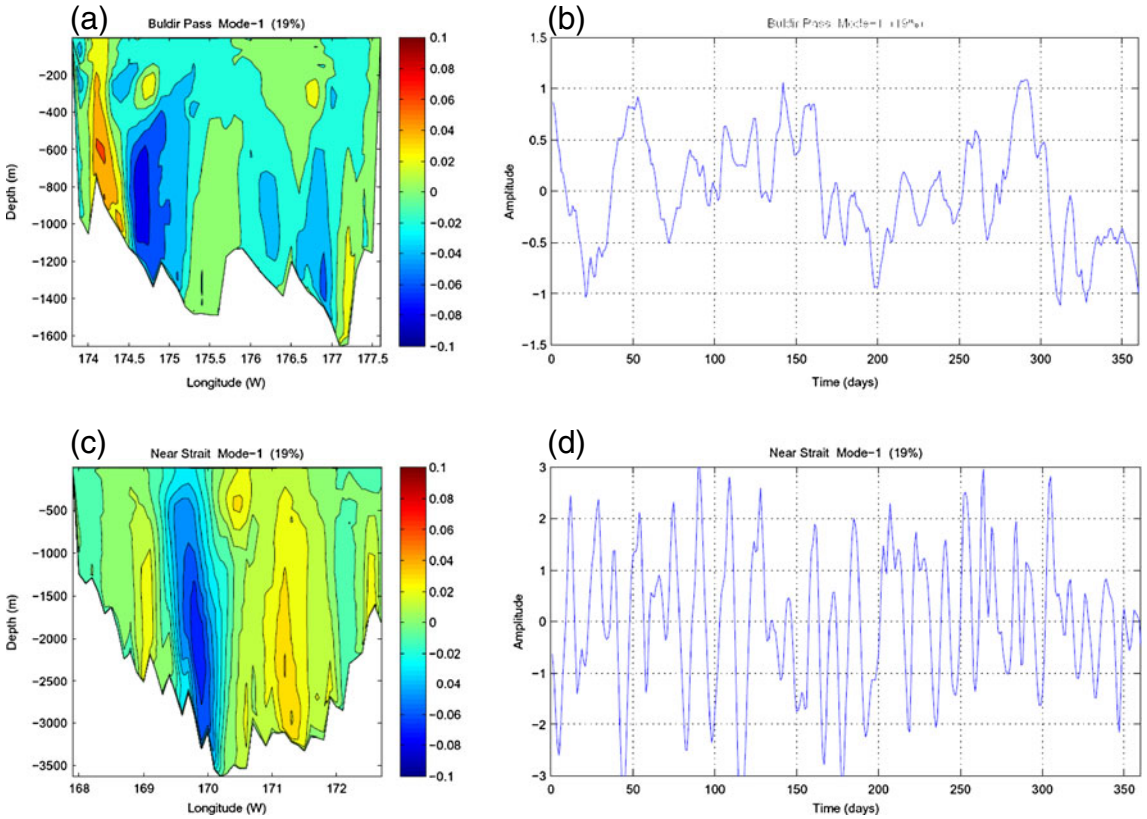

Fig. 11 The spatial (*left panels*) and temporal (*right panels*) pattern of the first EOF mode at Buldir Pass (*upper panels*) and Near Strait (*lower panels*). The EOFs of both straits contain exactly the same percent of the total variability (19 %), but with very different temporal frequencies

oscillations, and what mechanisms may potentially transfer the signal between straits located thousands of kilometers away from each other? To answer these questions, we look at two examples in which spectra of different straits are significantly coherent with each other (Fig. 12a–d).

Case 1: Bering strait–kamchatka strait connections These straits are connected through major ocean currents (e.g., KC) along the northwestern side of the BS (Figs. 1b and 2a), and variability in the BSC may influence both straits. The spectra of both straits have significant peaks of 13–14 and 32 days; at the former period, there is a significant coherency of 0.9 with ~5-day phase difference (Bering Strait leads) between the two spectra. The time series of the first two EOF modes of Kamchatka are linearly correlated to the Bering Strait mode-1 with correlation coefficient of 0.35 (95 % confidence level), but after applying a 30-day low-pass filter on the data, the correlation coefficient increases to 0.86 (at more than 99 % confidence level, Fig. 13a). Therefore, the deep-flow modes of Kamchatka Straits (Fig. 10d, e) seem to represent the low frequency deep transport variations. The EOF mode-3 of Kamchatka Straits, representing the surface variations of the KC (Fig. 10f), is also correlated with the Bering Strait mode-1 (Fig. 13b), with correlation coefficient of 0.25 (95 % confidence level) and 7-day phase difference; this mode seem to represent higher frequency surface variations. Note that it would take a few days for a barotropic wave traveling along the shallow coast of the BS to completely circle the BS. While evaluating all the basin-wide waves in the BS is beyond the scope of this study, the suggested mechanism involves eddy-induced changes in density and surface elevation that trigger barotropic and baroclinic waves which transfer the anomalies throughout the BS basin. In the next section, a potential source for these oscillations is proposed.

Case 2: Amchitka pass–amukta pass connections These two passages are located $\Delta X \sim 550$ km apart, in the central to eastern side of the Aleutian Arc (Fig. 1), between two strong currents, the westward flowing AS to the south and the eastward flowing ANSC to the north (Fig. 2). The most energetic signals are at a 43-day period (with 0.95 coherence between the two spectra and a ΔT=27-day phase difference; Fig. 12c, d). The signal at Amukta Pass leads that at Amchitka Pass, suggesting a westward propagating signal with speed of $c=\Delta X/\Delta T \sim 0.2$ ms^{-1}. Therefore, it is reasonable to hypothesize that the 43-day signal comes from mesoscale eddies and variability in the AS (Crawford et al. 2000; Maslowski et al. 2008). The time series of mode-1 in

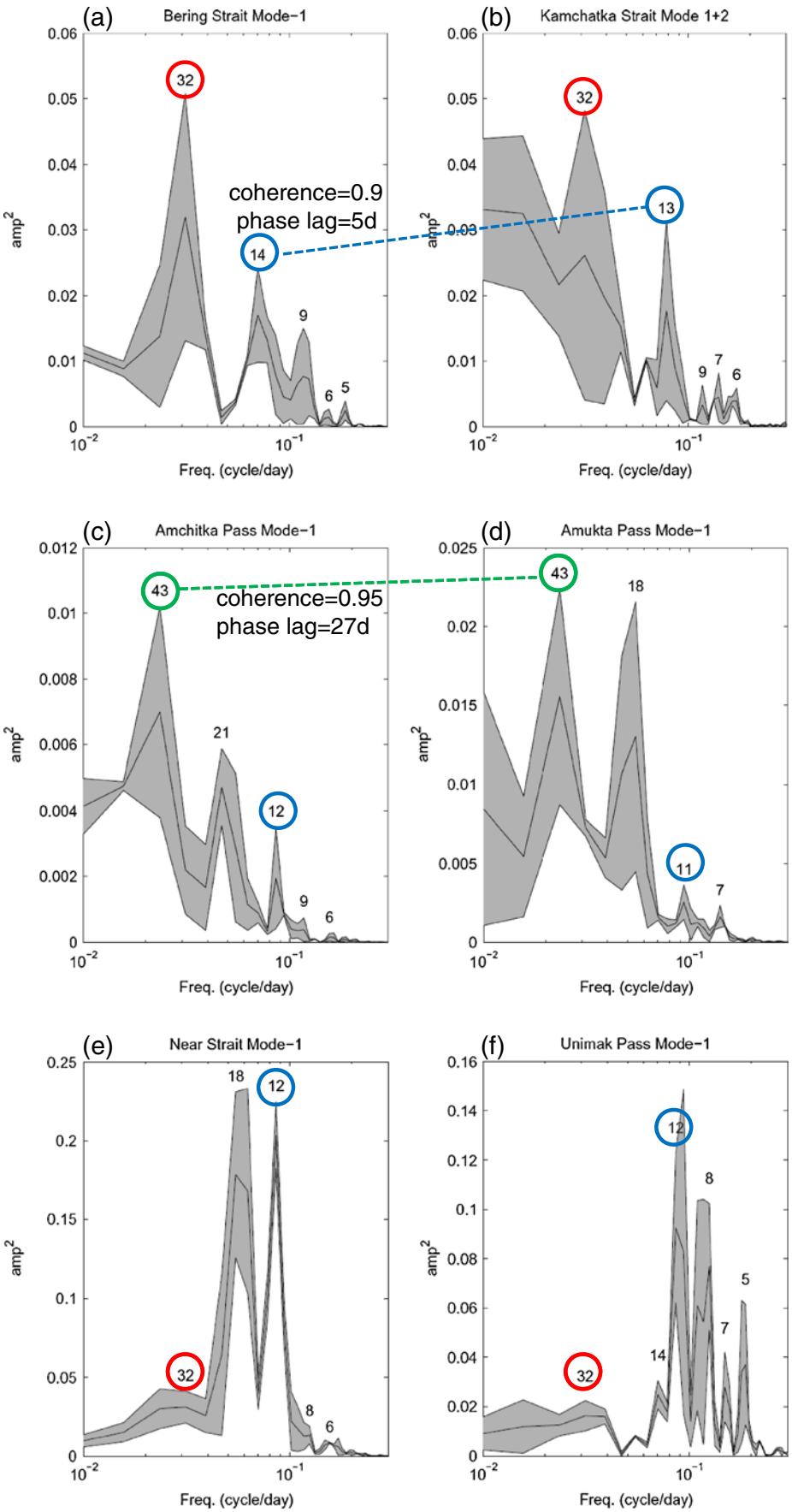

Fig. 12 Power spectra of EOF modes: (**a**) Bering Strait, (**b**) Kamchatka Strait, (**c**) Amchitka Pass, (**d**) Amukta Pass, (**e**) Near Strait, and (**f**) Unimak Pass; all are mode-1 except Kamchatka which combines modes-1 and -2. The *gray area* represents the 95 % confidence outline, and the *numbers* indicate period (in days) of the main peaks, with particular periods (see text) *highlighted by color circles*

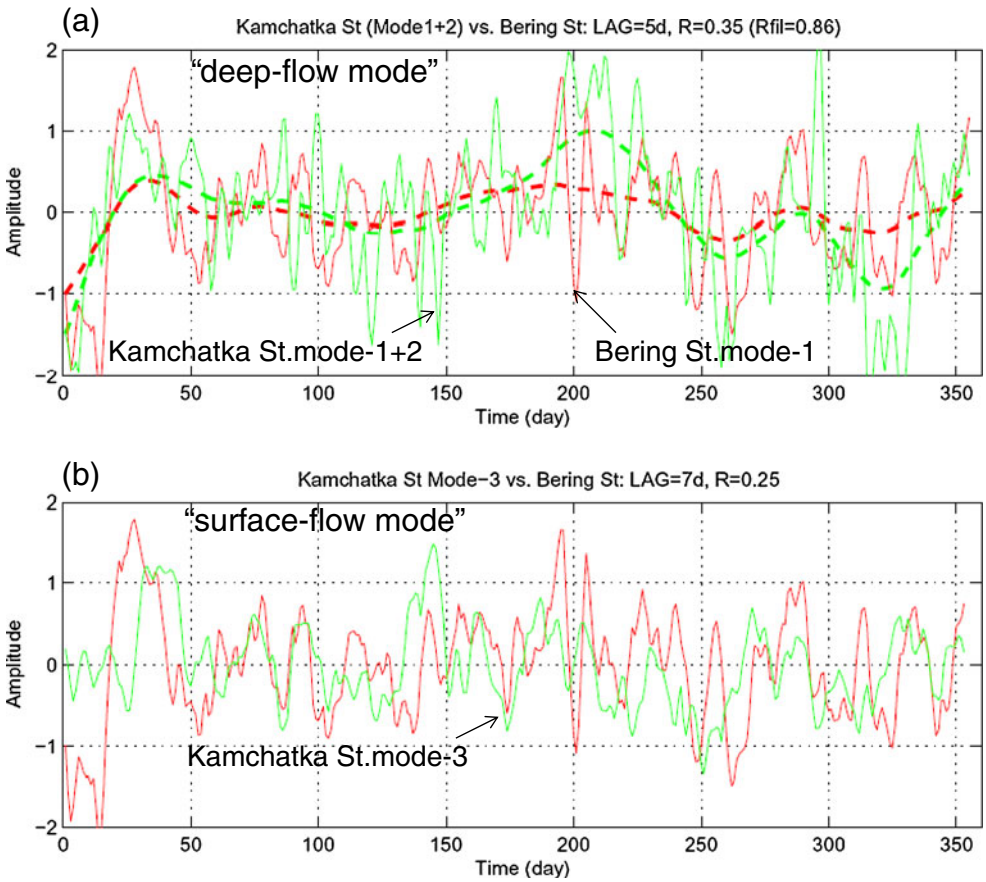

Fig. 13 Comparison of the time variation of Bering Strait's first EOF mode (*red lines* in **a** and **b**) with the Kamchatka EOF modes: (**a**) combined modes-1 and -2 (so-called "deep modes" in text), and (**b**) mode-3 (so-called "surface mode" in text). Lag and linear correlation coefficients are indicated (both correlations are significant at 95 % confidence level). Also shown in *heavy dash lines* in (**a**) are the low-pass filtered lines (correlation coefficient of 0.86 with larger than 99 % significance level)

these passages are shown in Fig. 14, indicating irregular eddy-like signals that propagate from Amukta to Amchitka passages within ~27 days (e.g., days 125, 270, and 320). The linear correlation coefficient between the two time series is 0.23 (95 % confidence level).

3.4 Bering sea-wide modes and sources of variability

The analysis of strait flows in the previous section clearly indicates some dominate modes of oscillations that can be seen at several straits located around the BS; future simulations with realistic forcing will be used for more detailed comparisons with observations. If these modes are propagating as fast-moving barotropic waves across the BS, variations in the sea surface height (SSH) in the model may give us some indication of the source of the variability (noting again that there are no time-dependent forcing in the model). Therefore, horizontal EOF modes from the daily SSH data were calculated and shown for the unforced case in Fig. 15. Let us look first at the relation between SSH oscillation periods (right panels of Fig. 15) and strait flow oscillations (Fig. 12). The most energetic SSH mode (EOF mode-1, with 73 % of the total variability, Fig. 15a) shows two regions of high energy, one along the east coast of Asia,

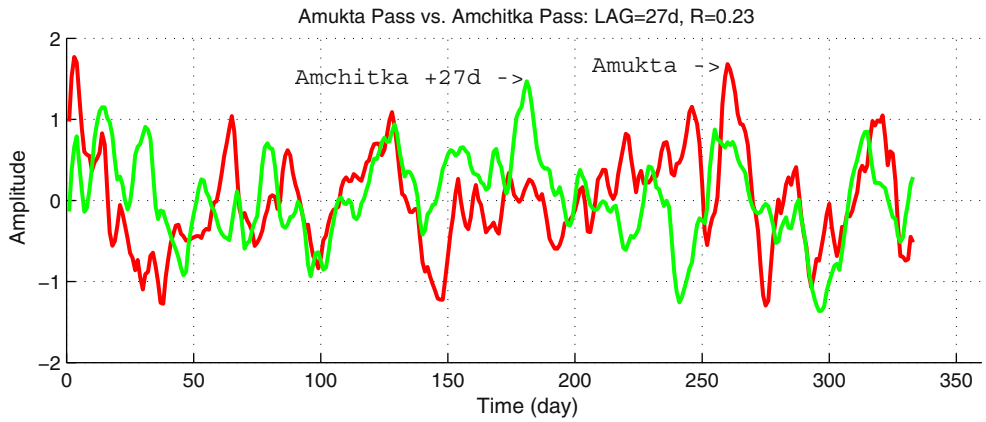

Fig. 14 The time variation of the first EOF mode of Amukta (*red line*) and Amchitka (*green line*) Passes, plotted with a 27-day lag (Amukta leads). Amchitka Pass is located ~550 km west of Amukta Pass (see Fig. 1)

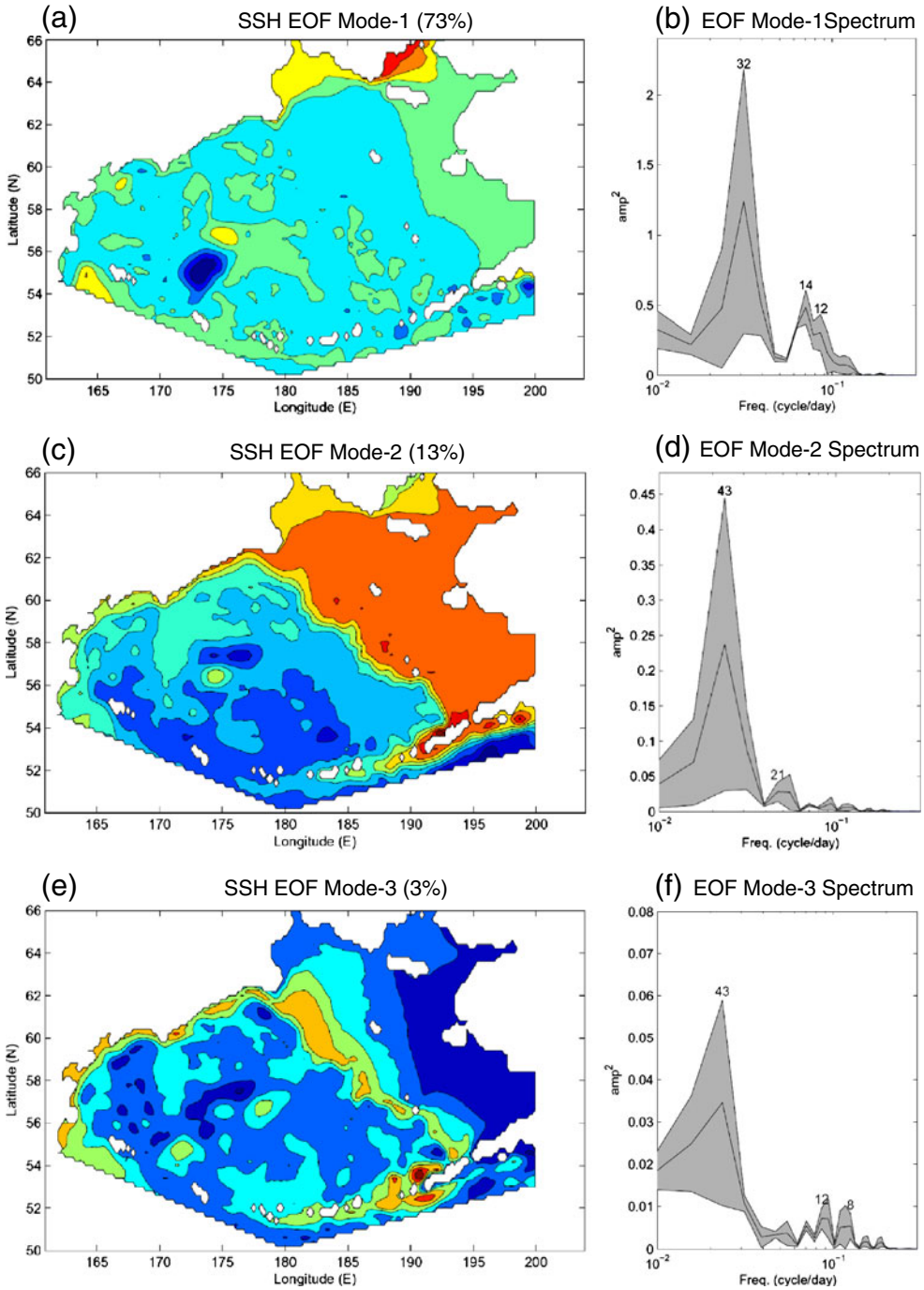

Fig. 15 The first three (*top to bottom*) EOF modes of Sea Surface Height (SSH) in the standard unforced case. *Left panels* are the horizontal spatial pattern (*red* and *blue* are in opposite phase with the maximum–minimum range indicated, *green* is around zero; percent of total variability is also indicated), and *right panels* are the spectra of the time-dependent amplitude of each mode

south of the Bering Strait, and one in the Aleutian Basin, near the Bowers Ridge. This mode is associated with oscillations with periods of 32 and 14 days (Fig. 15b), similar to the period of oscillations seen in the Bering Strait and the Kamchatka Strait (Fig. 12a, b).

Although EOF modes-2 and -3 of SSH represent only small portion of the total variability over the entire BS (13 % and 3 %, respectively; Fig. 15c, e), they represent large portion of the variability in the southeastern region of the domain. The maximum variability in these two modes is focused near the Alaskan Stream east of 190°E, and the dominant period of oscillations is at T=43 days (Fig. 15d, f). This analysis confirms our previous hypothesis that the 43-day variability seen at Amukta, Amchitka, and Buldir Passages (Fig. 12) is related to the AS. Mode-2 (Fig. 15c) shows an opposite phase between the Bering Shelf and the Aleutian Basin. The two basins are separated by the BSC (BSC, Fig. 1b), so a change in the strength of the geostrophic current would be associated with a change in SSH on both sides of the current. This suggests a mechanism in which the

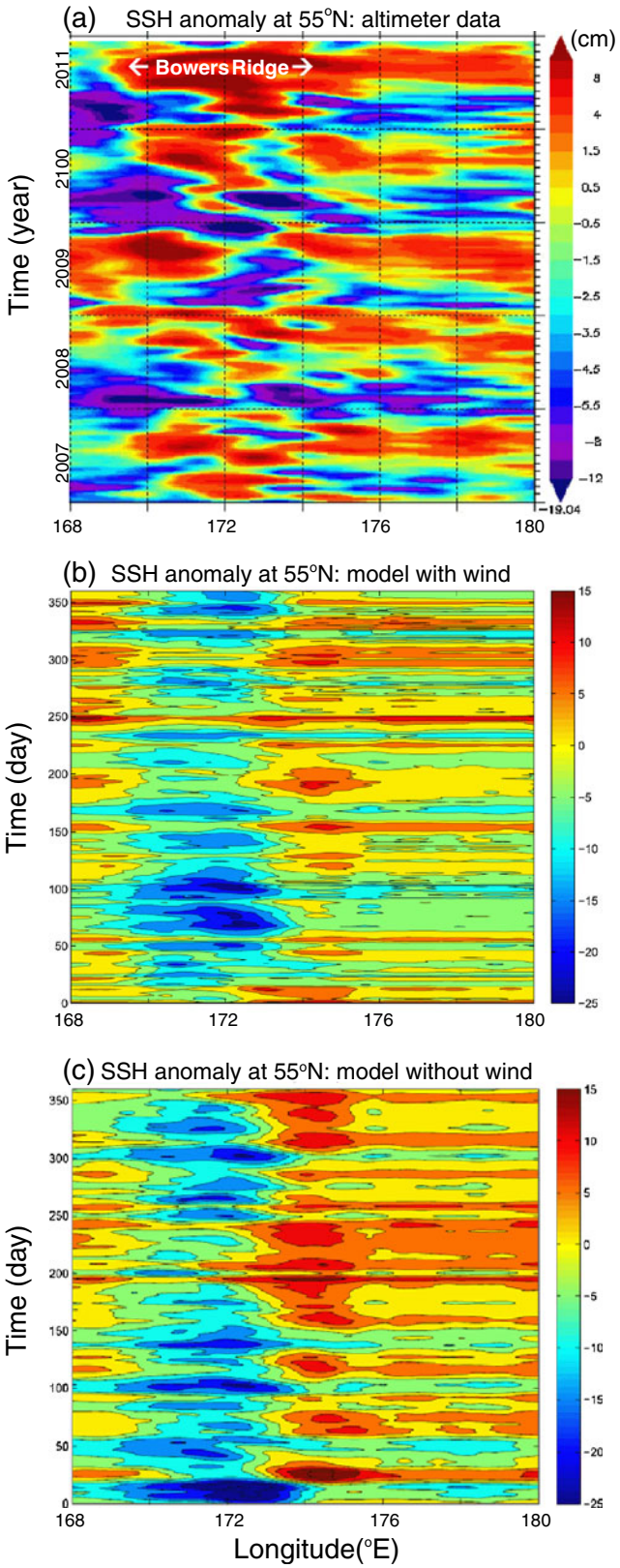

Fig. 16 **a** Five years of sea surface height anomaly from altimeter data across 55°N as a function of longitude and time; (**b**) and (**c**) are similar plots, but for 1-year of model simulations with and without wind, respectively. Note the high anomaly across the Bowers Ridge in the observations and the model simulations

AS may influence the Bering Strait transport: strengthening of the AC and BSC would result in lowering SSH over the Aleutian Basin and increasing SSH over the Bering Shelf, which in turn creates larger pressure gradient between the BS and the Arctic, driving more flow through the Bering Strait. Mode-3, with maximum variability east of Amukta Pass and all along the BSC and the southeastern coast of Siberia, may be due to AS eddies that cause BSC mesoscale variability along the Bering slope and the western coast of the BS.

The SSH EOF mode-1 suggests a source of variability in the deep Aleutian Basin (Fig. 15a). However, since there is no surface forcing in the standard simulation, what is the mechanism that can generate this variability? The hypothesis is that this variability is generated by the interaction of currents and mesoscale eddies with the steep slopes of the Bowers Ridge (Figs. 1b and 2a). Bottom steering by this ridge is also seen in observations and model simulations (Wang et al. 2009). To verify this hypothesis, SSH anomaly from 5 years of altimeter data (Ducet et al. 2000) across 55°N (over the Bowers Ridge) is analyzed and shown in Fig. 16a (in the form known as a Hovmöller diagram). In comparison, Fig. 16b, c shows similar diagrams from 1 year of the model simulations with and without wind, respectively. Both model runs and the data clearly show significant SSH anomalies (eddies?) over the Bowers Ridge region that are different than the pattern of SSH seen elsewhere away from the ridge. This area of increased variability is exactly the area in Fig. 15a that the EOF mode-1 of the model SSH indicates maxima in variability. The close similarity between the two model simulations with or without wind indicates that the flow–topography interaction over the Bowers Ridge is the source of the observed variability and not the wind. In fact, the addition of high-frequency wind in the model slightly reduces the variability in those longer mesoscale periods, which may be by enhancing the upper ocean mixing. The importance of the Bowers Ridge to the BS variability may be attributed to the fact that it is a dominant topographic feature that disturbs the flow in the deep basin; most of the other major currents are coastally trapped around the BS edges, generally flowing along the bathymetry lines so they may not generate as much variability as currents that cross isobathic lines.

4 Summary and conclusions

An idealized, high-resolution numerical ocean model of the BS was used as a tool to study the dynamics of strait flows and to shed light on sources of mesoscale variability in the BS. In the unforced standard case, the model has realistic topography, but has no external forcing except constant inflows/outflows imposed on its boundaries—this allows us to isolate internally generated modes of variability from

forced one (e.g., seasonal and high-frequency wind patterns and tidal cycles). Despite the idealized forcing, the major ocean currents of the BS are reproduced, as well as a rich eddy variability field.

By comparing the flow through six Aleutian passages and the Bering Strait, some general conclusions can be drawn about the strait dynamics, which may be applicable to other straits. The BS straits range in depth from ~50 to ~4,500 m and in width from ~50 to ~500 km, so they cover a large range of topographies. A set of basic parameters that describe the strait topography, stratification, stability, baroclinicity, etc. were estimated and summarized in Table 1. EOF analysis of the flow through each strait identified the main modes of variability. An interesting finding was that strait variability monotonically increases with increasing barotropic and baroclinic Rossby Radii of Deformations, independent of forcing and geographical location (Fig. 5).

Three general types of distinct strait dynamics were identified, based on the aspect ratio (s=width/depth) and depth (H), "Shallow" straits (s>500; H<100 m), "Deep" straits (s<100; H>1,500 m), and "Wide" straits (100<s<500; 750 m<H; L>250 km):

1. "Shallow" passages include the Bering Strait and the Unimak Passage; they have near barotropic flows with maximum transport at a fixed location. Without external forcing, over 90 % of the flow variability is contained in a single EOF mode representing variations in the total transport. High-frequency oscillations with periods of ~5–10 days are believed to be generated in the Unimak Pass due to a local instability associated with super critical flows (Froude number, Fr>1). It is interesting to compare the results here with the modeling study of the Faroe Bank Channel by Ezer (2006), who found that observed 5-day period oscillations in FBC can be explained by strait instability. Although the FBC in the North Atlantic Ocean is a two-layer system with much stronger stratification than the BS straits, topographically, it is a relatively narrow strait with small aspect ratio (s~25), and it has supercritical flows with Fr near or over 1, similar to the Unimak Pass and the Bering Strait.
2. "Deep" straits include Amchitka Pass and Kamchatka Strait; they have major surface currents at the western side of the strait and deep flows along the slopes of the strait. Although these two straits have different temporal variability (Fig. 12b, c), and different geographical setting and circulation patterns (Fig. 1), their mean flow patterns are very similar (Fig. 7a, c), indicating the dominant role that the local topography plays. In comparison, the flows in those straits resemble to some extent the flow observed and modeled in the relatively deep (H~2,000 m) Yucatan Channel (Ezer et al. 2003; Oey et al. 2004). Long-term, deep observations are clearly needed in the Amchitka and Kamchatka straits to verify the nature of the deep flows found in the model, but it is interesting to note that in the YC case, the locations of deep return flows were first identified by models, and only later observations were available to confirm the model findings (see Ezer et al. 2003, for review of observations and models in the YC).
3. "Wide" passages includes Near Straits, Amukta Pass, and Buldir Pass; they have complex flow patterns modulated by mesoscale eddies. Amukta and Buldir Passes are influenced by westward propagating meanders and eddies with periods of ~43 days, associated with the AS south of the straits, while Near Strait is affected by eastward propagating eddies in the Aleutian Basin itself, north of the strait, with periods of 12–18 days.

Significant coherence (but with phase shifts) between oscillations found at different straits located hundreds to thousands of kilometers from each other suggests that signals propagate as fast-moving barotropic and coastal waves throughout the BS. Two sources of variability were indentified from EOF analysis of sea surface height variability. The first source, with a dominant 43-day period, is in the western Alaskan Stream. The signal seems to have the most impact on the Amukta, Amchitka, and Buldir straits along the Aleutian Arc. This variability also affects the strength and position of the BSC and the KC at the western side of the Aleutian Basin. Observations (e.g., Reed and Stabeno 1993; Stabeno et al. 2005; Ladd and Stabeno 2009) have previously shown that the AS strongly impact the flow through the Aleutian passages, but the model helps explain the detail of the mechanism involved. If the impact of the AS on the SSH over the Bering Shelf (Fig. 15c) is correct, it may have implications for the BS–Arctic pressure difference and transports through the BS. A second source of variability with periods of 14 and 32 days (Fig. 15a, b) has a local origin in the Aleutian Basin and resulted from the interaction of currents with the steep slopes of the Bowers Ridge. In the case without input from wind variability, this mode is responsible for the majority of the total variability in the BS. Altimeter data (Fig. 16) confirms that this region near the Bowers Ridge is in fact a very energetic region with SSH anomalies of ~10–20 cm amplitude that are larger than the seasonal variations.

In this process-oriented study, only limited comparisons have been made between the unforced case and a wind-driven simulation and between model results and observations (for realistic simulations of the BS and model–data comparisons, using a similar dynamical model, see, for example, Wang et al. 2009 and Hu and Wang 2010). Nevertheless, comparisons of the two model runs suggest that flow–topography interactions play important roles in deep strait flows and in generating variability over oceanic ridges, independent of wind. The implication is that some

natural modes of variability are intrinsic to the BS topography and can be excited by various forcing such as mesoscale variations in the Alaskan Stream.

In summary, while the idealized model study is useful in revealing basic dynamical processes that otherwise may have been masked by variability associated with tides, winds, and sea ice formation, supporting studies using more realistic forcing are also needed. Observations can be used in the future to verify some of the model findings, in particular, the flow patterns in deep passages.

Acknowledgments The research is supported by NOAA's Office of Climate Programs, through grants to ODU (award NA08OAR4310613) and PU (award NA17RJ2612), as part of the project "Collaborative Research: Modeling Sea Ice-Ocean-Ecosystem Responses to Climate Changes in the Bering-Chukchi-Beaufort Seas with Data Assimilation of RUSALCA Measurements." TE was partly supported by grants from NSF and NOAA. LYO is grateful to GFDL/NOAA, Princeton, where model computations were conducted.

References

Aagaard K, Roach AT, Schumacher JD (1985) On the wind-driven variability of the flow through Bering Strait. J Geophys Res 90 (C10):7213–7222

Bretherton CS, Smith C, Wallace JM (1992) An intercomparison of methods for finding coupled patterns in climate data. J Clim 5:541–560

Cenedese C, Whitehead JA, Ascarelli TA, Ohiwa M (2004) A dense current flowing down a sloping bottom in a rotating fluid. J Phys Oceanogr 34:188–203

Coachman LK, Aagaard K (1988) Transports through Bering Strait: annual and interannual variability. J Geophys Res 93(C12):15,535–15,539

Crawford WR, Cherniawsky JY, Foreman MGG (2000) Multi-year meanders and eddies in the Alaskan Stream as observed by TOPEX/Poseidon altimeter. Geophys Res Lett 27(7):1025–1028

De Boer AM, Nof D (2004) The Bering Strait's grip on the northern hemisphere climate. Deep-Sea Res 51:1347–1366

Ducet N, Le Traon PY, Reverdin G (2000) Global high-resolution mapping of ocean circulation from TOPEX/Poseidonand ERS1 and 2. J Geophys Res 105(C8):19477–19498. doi:10.1029/2000JC900063

Ezer T (2006) Topographic influence on overflow dynamics: Idealized numerical simulations and the Faroe Bank Channel overflow. J Geophys Res 111(C02002). doi:10.1029/2005JC003195

Ezer T, Oey L-Y (2010) The role of the Alaskan Stream in modulating the Bering Sea climate. J Geophys Res C04025. doi:10.1029/2009JC005830

Ezer T, Oey L-Y, Lee H-C, Sturges W (2003) The variability of currents in the Yucatan Channel: analysis of results from a numerical ocean model. J Geophys Res 108(C1):3012. doi:10.1029/2002JC001509

Favorite F (1967) The Alaskan Stream. Int N Pac Fish Comm Bull 21:20

Favorite F (1974) Flow into the Bering Sea through Aleutian Island passages. In: Hood DW, Kelley EJ (eds) Oceanography of the Bering Sea with emphasis on renewable resources. Publication No. 2. Institute of Marine Science, University of Alaska, Fairbanks, pp. 3–37

Foreman MGG, Cummins PF, Cherniawsky JY, Stabeno P (2006) Tidal energy in the Bering Sea. J Mar Res 64:797–818. doi:10.1357/002224006779698341

Hu H, Wang J (2010) Modeling effects of tidal and wave mixing on circulation and thermohaline structures in the Bering Sea: process studies. J Geophys Res 115(C01006). doi:10.1029/2008JC005175

Hunt GL Jr, Stabeno P, Walters G, Sinclair E, Brodeur RD, Napp JM, Bond NA (2002) Climate change and control of the southeastern Bering Sea pelagic ecosystem. Deep-Sea Res 49:5821–5853

Jin M, Deal C, Wang J, McRoy CP (2009) Response of lower trophic level production to long-term climate change in the southeastern Bering Sea. J Geophys Res 114(C04010). doi:10.1029/2008JC005105

Johnson GC, Stabeno PJ, Riser SC (2004) The Bering slope current system revisited. J Phys Oceanogr 34:384–398

Ladd C, Stabeno PJ (2009) Freshwater transport from the Pacific to the Bering Sea through Amukta Pass. Geophys Res Lett 36(L14608). doi:10.1029/2009GL039095

Legg S, Chang Y, Chassignet EP, Danabasoglu G, Ezer T, Gordon AL, Griffies S, Hallberg R, Jackson L, Large W, Ozgokmen T, Peters H, Price J, Riemenschneider U, Wu W, Xu X, Yang J (2009) Improving oceanic overflow representation in climate models: the Gravity Current Entrainment Climate Process Team. Bull Amer Met Soc 90 (5):657–670

Liu SK, Leendertse JJ (1982) Three-dimensional model of Bering and Chukchi Sea. Coastal Eng 18:598–616

Maslowski W, Roman R, Kinney JC (2008) Effects of mesoscale eddies on the flow of the Alaskan Stream. J Geophys Res 113 (C07036). doi:10.1029/2007JC004341

Mellor GL (2004) Users' guide for a three-dimensional, primitive equation, numerical ocean model. Prog Atmos Oceanic Sci, Princeton University, Princeton, p 42

Mellor GL, Yamada T (1982) Development of a turbulent closure model for geophysical fluid problems. Rev Geophys Space Phys 20:851–875

Ochoa J, Sheinbaum J, Baden A, Candela J, Wilson D (2001) Geostrophy via potential vorticity inversion in the Yucatan Channel. J Mar Res 59:725–747

Oey LY, Ezer T, Sturges W (2004) Modeled and observed Empirical Orthogonal Functions of currents in the Yucatan Channel. J Geophys Res 109(C08011). doi:10.1029/2004JC002345

Overland JE, Spillane MC, Hurlburt HE, Wallcraft AJ (1994) A numerical study of the circulation of the Bering Sea basin and exchange with the North Pacific Ocean. J Phys Oceanogr 24:736–758

Panteleev G, Stabeno P, Luchin VA, Nechaev DA, Ikeda M (2006) Summer transport estimates of the Kamchatka Current derived as a variational inverse of hydrophysical and surface drifter data. Geophys Res Lett 33(L09609). doi:10.1029/2005GL024974

Pickart RS, Moore GWK, Macdonald AM, Renfrew IA, Walsh JE, Kessler WS (2009) Seasonal evolution of Aleutian low pressure systems: implications for the North Pacific subpolar circulation. J Phys Oceanogr 39:1317–1339

Reed RK (1968) Transport of the Alaskan Stream. Nature 220(16):681–682

Reed RK (1984) Flow of the Alaskan Stream and its variations. Deep-Sea Res 31(4):369–386

Reed RK (1990) A year-long observation of water exchange between the North Pacific and the Bering Sea. Limnol Oceanogr 35 (7):1604–1609

Reed RK, Stabeno PJ (1993) The recent return of the Alaskan Stream to Near Strait. J Mar Res 51:515–527

Reed RK, Stabeno PJ (1999) A recent full-depth survey of the Alaskan Stream. J Oceanogr 55:79–85

Roach AT, Aagaard K, Pease CH, Salo SA, Weingartner T, Pavlov V, Kulakov M (1995) Direct measurements of transport and water properties through the Bering Strait. J Geophys Res 100 (C9):18,443–18,457

Royer TC (1975) Seasonal variations of waters in the northern Gulf of Alaska. Deep-Sea Res 22:403–416

Royer TC, Emery WI (1984) Circulation in the Bering Sea, 1982–1983, based on satellite-tracked drifter observations. J Phys Oceanogr 14:1914–1920

Sheinbaum J, Candela J, Badan A, Ochoa J (2002) Flow structure and transports in the Yucatan Channel. Geophys Res Lett 29(3). doi:10.1029/2001GL0139990

Stabeno PJ, Reed R (1992) A major circulation anomaly in the western Bering Sea. Geophys Res Lett 19(16):1671–1674

Stabeno PJ, Kachel DG, Kachel NB, Sullivan ME (2005) Observations from moorings in the Aleutian Passes: temperature, salinity and transport. Fisheries Oceanogr 14(1):39–54

Stabeno PJ, Ladd C, Reed RK (2009) Observations of the Aleutian North Slope Current, Bering Sea, 1996–2001. J Geophys Res 114 (C05015). doi:10.1029/2007JC004705

Stabeno PJ, Schumacher JD, Ohtani K (1999) The physical oceanography of the Bering Sea. In: Loughlin TR, Ohtani K (eds) Dynamics of the Bering Sea. University of Alaska Sea Grant AK-SG-99-03, Fairbanks, pp. 1–28

Thomson RE (1972) On the Alaskan stream. J Phys Oceanogr 2(4):363–371

Wang J, Hu H, Mizobata K, Saitoh S (2009) Seasonal variations of sea ice and ocean circulation in the Bering Sea: a model-data fusion study. J Geophys Res 114(C02011). doi:10.1029/2008JC004727

Woodgate RA, Aagaard K, Weingartner TJ (2005) Monthly temperature, salinity, and transport variability of the Bering Strait through flow. Geophys Res Lett 32(L04601). doi:10.1029/2004GL021880

Woodgate RA, Aagaard K, Weingartner TJ (2006) Interannual changes in the Bering Strait fluxes of volume, heat and freshwater between 1991 and 2004. Geophys Res Lett 33(L15609). doi:10.1029/2006GL026931